Research in Astronomy and Astrophysics, 25:015018 (13pp), 2025 January
https://doi.org/10.1088/1674-4527/ada2e9
CSTR: 32081.14.RAA.ada2e9

Producing Type Ia Supernovae from Hybrid CONe White Dwarfs with Main-sequence Binary Companions at Low Metallicity of $Z = 0.0001$

Boyang Guo[1,2,3,4], Xiangcun Meng[1,2], Zhijia Tian[3], Jingxiao Luo[1,2,4], and Zhengwei Liu[1,2]
[1] Yunnan Observatories, Chinese Academy of Sciences (CAS), Kunming 650216, China; zwliu@ynao.ac.cn
[2] International Centre of Supernovae (ICESUN), Yunnan Key Laboratory, Kunming 650216, China
[3] Department of Astronomy, Key Laboratory of Astroparticle Physics of Yunnan Province, Yunnan University, Kunming 650500, China
[4] University of Chinese Academy of Sciences, Beijing 100049, China
Received 2024 September 30; revised 2024 December 03; accepted 2024 December 16; published 2025 January 16

Abstract

The nature of progenitors of Type Ia supernovae (SNe Ia) and their explosion mechanism remains unclear. It has been suggested that SNe Ia may have resulted from thermonuclear explosions of hybrid carbon–oxygen–neon white dwarfs (CONe WDs) when they grow in mass to approach the Chandrasekhar mass limit by accreting matter from a binary main-sequence (MS) companion. In this work, we combine the results of detailed binary evolution calculations with population synthesis models to investigate the rates and delay times of SNe Ia in the CONe WD + MS channel at a low metallicity environment of $Z = 0.0001$. For a constant star formation rate of $5\,M_{\odot}\,\mathrm{yr}^{-1}$, our calculations predict that the SN Ia rates in the CONe WD + MS channel at low metallicity of $Z = 0.0001$ is about $0.11-3.89 \times 10^{-4}\,\mathrm{yr}^{-1}$. In addition, delay times in this channel cover a wide range of 0.05−2.5 Gyr. We further compare our results to those given by a previous study for the CONe WD + MS channel with a higher metallicity of $Z = 0.02$ to explore the influence of metallicity on the results. We find that these two metallicity environments give a slight difference in rates and delay times of SNe Ia from the CONe WD + MS channel, although SNe Ia produced at a low metallicity environment of Z = 0.0001 have relatively longer delay times.

Key words: methods: numerical – (stars:) binaries (including multiple): close – stars: evolution – (stars:) supernovae: general – (stars:) white dwarfs

1. Introduction

Type Ia supernovae (SNe Ia) are the cataclysmic explosions of intermediate-mass stars at the end of their lives. SNe Ia have typical *B*-band peak magnitudes of around −19.5 mag, which are as bright as their host galaxies. SNe Ia have been used as the standard candles to measure cosmological parameters due to the high luminosities and homogeneity of their light curves (Riess et al. 1998; Perlmutter et al. 1999). SNe Ia are one of the main contributors to heavy-elements such as intermediate-mass and iron-group elements in the Universe (e.g., Matteucci & Greggio 1986). Despite of the importance of SNe Ia, their progenitors and explosion mechanism remain a mystery (see Maoz et al. 2014; Livio & Mazzali 2018; Jha et al. 2019; Liu et al. 2023, for recent reviews).

It is widely accepted that SNe Ia may be originated from thermonuclear explosions of carbon–oxygen white dwarfs (CO WDs) in binary systems (e.g., Hoyle & Fowler 1960; Nomoto 1982; Nomoto et al. 1984; Bloom et al. 2012). Depending on the nature of donor stars, different progenitor models have been proposed for SNe Ia, including the single-degenerate (SD) scenario (e.g., Whelan & Iben 1973; Nomoto et al. 1984; Han & Podsiadlowski 2004), the double-degenerate (DD) scenario (e.g., Iben & Tutukov 1984; Webbink & Iben 1987), the core-degenerate scenario (e.g., Livio & Riess 2003; Kashi & Soker 2011; Ilkov & Soker 2012; Soker et al. 2013, 2014; Soker 2018), the triple model (e.g., Katz & Dong 2012; Hamers et al. 2013; Toonen et al. 2018; Rajamuthukumar et al. 2023) and the single star model (e.g., Iben & Renzini 1983; Tout 2005; Antoniadis et al. 2020), etc. In this work, we will focus only on the SD scenario. In the SD scenario, the WD accretes material from its non-degenerate companion star to accumulate mass on its surface, triggering a thermonuclear explosion when the WD grows in mass to approach the Chandrasekhar-mass limit. The donor star in this scenario could be a main-sequence (MS) star, a sub-giant star, a red giant (RG) star or a helium (He) star (e.g., Hachisu et al. 1999; Han & Podsiadlowski 2004; Meng et al. 2009; Ruiter et al. 2009; Wang et al. 2009; Meng & Yang 2010; Liu & Stancliffe 2018, 2020).

The SD scenario has advantages and disadvantages in both theoretical and observational sides, which have been comprehensively reviewed by Liu et al. (2023). We therefore only briefly summarize them here. The SD scenario seems likely to explain the homogeneity of peak luminosities of the so-called normal SNe Ia because that the WDs in this scenario are expected to explode near the Chandrasekhar-mass limit. However, only a narrow range of mass-transfer rates can lead to a stable mass accumulation onto the WD in the SD scenario.

This leads to the predicted SN Ia rates in this scenario have difficulties in explaining those inferred from observations (e.g., Paczynski 1976; Fujimoto 1982a, 1982b; Livio et al. 1989; Han & Podsiadlowski 2004; Nomoto et al. 2007; Shen & Bildsten 2007; Meng et al. 2009; Ruiter et al. 2009; Wang et al. 2009; Meng & Yang 2010; Wolf et al. 2013; Claeys et al. 2014; Piersanti et al. 2014; Liu & Stancliffe 2018; Liu et al. 2023). On the observational side, there are certain observations seem to suggest that some SNe Ia may be produced from the SD scenario. For instance, McCully et al. (2014) reported that a blue luminous source was detected in the pre-explosion image of an SN Iax event,[5] SN 2012Z. This blue luminous source has been thought to be a He star companion of its progenitor system. Also, some studies reported that the narrow absorption signatures of circumstellar material that are thought to be originated from the mass-transfer from the companion stars in the SD scenario have been detected in some SNe Ia (e.g., Patat et al. 2007; Sternberg et al. 2011; Dilday et al. 2012; Silverman et al. 2013; but see also Soker et al. 2013). However, no promising surviving companion star predicted by the SD scenario has been firmly confirmed yet in nearby SN remnants (SNRs; Kerzendorf et al. 2009; Schaefer & Pagnotta 2012; Ruiz-Lapuente et al. 2018), although there are a few candidates such as Tycho G (Ruiz-Lapuente et al. 2004, 2019; Fuhrmann 2005; Ihara et al. 2007; González Hernández et al. 2009; Kerzendorf et al. 2009, 2013; Bedin et al. 2014; Ruiz-Lapuente 2023a), US 708 (Geier et al. 2015; Bauer et al. 2019; Liu et al. 2021) and MV-G272 (Ruiz-Lapuente et al. 2023). The features of swept-up H/He due to the SN ejecta-companion interaction predicted by hydrodynamical models have not been firmly confirmed by the observations yet (e.g., Marietta et al. 2000; Pakmor et al. 2008; Liu et al. 2012, 2013; Pan et al. 2012; Boehner et al. 2017; McCutcheon et al. 2022), although there are a few candidate objects show H/He emission lines in their late-time spectra (Leonard 2007; Lundqvist et al. 2013, 2015; Shappee et al. 2013, 2018; Maguire et al. 2016; Graham et al. 2015, 2017; Dimitriadis et al. 2017, 2019; Hosseinzadeh et al. 2017, 2022; Sand et al. 2018, 2019, 2021; Holmbo et al. 2019; Jacobson-Galán et al. 2019; Tucker et al. 2019, 2020, 2022; Vallely et al. 2019; Prieto et al. 2020; Siebert et al. 2020; Elias-Rosa et al. 2021). In addition, the lack of X-ray emission in current observations (see Meng & Han 2016, e.g., Horesh et al. 2012; Margutti et al. 2014) also seems to challenge the SD scenario.

A series of previous studies on the SD scenario generally assumed that the accreting WD is a carbon–oxygen (CO) WD (e.g., Hoyle & Fowler 1960; Nomoto et al. 1984; Hachisu et al. 1999; Han & Podsiadlowski 2004; Meng et al. 2009; Ruiter et al. 2009; Claeys et al. 2014; Wang et al. 2014; Liu & Stancliffe 2018). Based on stellar evolution calculations, Denissenkov et al. (2013) found that a CO core that goes through an off-centered C-ignition in an asymptotic giant branch (AGB) star can stall its C-burning due to the convective boundary mixing. As a result, the AGB star would eject its envelope after the core nuclear reaction, leaving a hybrid CO-neon (Ne) WD consisting of a CO core and an ONe mantle (Denissenkov et al. 2013). Furthermore, Chen et al. (2014) suggest that the hybrid carbon–oxygen–neon white dwarfs (CONe WD) could be as massive as $1.3\,M_{\odot}$ at a low value of the C-burning rate (CBR) factor of 0.1.[6] Such massive CONe WDs have been thought to likely accrete a small amount of mass from their companion stars to reach the Chandrasekhar-mass limit to trigger SN Ia explosions if they are in binary systems (Denissenkov et al. 2015). Therefore, some previous studies have proposed the binary systems composed of a hybrid CONe WD and a non-degenerate companion star as a new subtype of SD progenitor model for SNe Ia (e.g., García-Berro et al. 1997; Denissenkov et al. 2013, 2015; Chen et al. 2014; Meng & Podsiadlowski 2014; Wang et al. 2014; Kromer et al. 2015; Liu et al. 2015; Marquardt et al. 2015). Recently, Kromer et al. (2015) have shown that the incomplete off-center pure deflagration explosions of near-Chandrasekhar-mass hybrid CONe WDs (sometimes known as "failed-detonation model"; see also Jordan et al. 2012; Kromer et al. 2013; Fink et al. 2014; Lach et al. 2022) could provide reasonable agreement with the observational features of faint Type Iax SN 2008ha. However, whether the convective boundary mixing could be strong enough to stall the c-burning inside AGB stars remains open (see Lecoanet et al. 2016; Lattanzio et al. 2017).

By performing binary population synthesis (BPS) calculations, Meng & Podsiadlowski (2014) and Wang et al. (2014) have respectively investigated the rates and delay times of SNe Ia produced from thermonuclear explosions of near-Chandrasekhar-mass hybrid CONe WDs with an MS donor (i.e., CONe WD + MS channel) and/or a He star donor (i.e., CONe WD + He star channel). Depending on different initial conditions and assumptions in their BPS calculations, both works have suggested SN Ia rates from near-Chandrasekhar-mass hybrid CONe WDs to be of the order of a few per cent of the Galactic SN Ia rates (Meng & Podsiadlowski 2014; Wang et al. 2014). In addition, because hybrid CONe WDs are expected to form through relatively massive zero-age MS stars (ZAMS; Chen et al. 2014), they found that this scenario could partly explain the short delay times of SNe Iax. However, these studies focused only on cases with solar-like metallicity (i.e., $Z = 0.02$). It is unclear how different metallicities affect the SN Ia rates and delay times in the SD scenario with accreting hybrid CONe WDs. In particular, the observations have detected SNe Ia with a high redshift of $z > 2$ (Rodney et al. 2014, 2015; Williams et al. 2020; Hayden et al. 2021; Pierel et al. 2024), which seems

[5] SN Iax is a subclass of SN Ia with sub-luminosity and lower expansion velocity (Li et al. 2003; Foley et al. 2013).

[6] The CBR factor characterizes the difficulty of C-ignition in the CO core of an AGB star (Denissenkov et al. 2013; Chen et al. 2014).

to indicate the production of SNe Ia at lower-metallicity environments.

In this work, we investigate the SNe Ia generated from the CONe WD + MS channel at low metallicity of $Z = 0.0001$ by combining the results of detailed binary evolution into population synthesis calculations. We aim to study the effect of different metallicities on the SN Ia rates and delay times in the CONe WD + MS channel. The paper is organized as follows: we describe the models and methods used in this work in Section 2. The results given by our detailed binary evolution and BPS calculations are presented in Section 3. Our discussions are shown in Section 4. Finally, we summarize our results in Section 5.

2. Methods

2.1. Binary Evolution Calculation

In this work we use the same method adopted by Han & Podsiadlowski (2004) to predict the rates and delay times of SNe Ia produced from the hybrid CONe WD + MS channel at a low metallicity environment, in which the results of detailed binary evolution calculations are combined with population synthesis models. We use the stellar evolution code `Modules for Experiments in Stellar Astrophysics` (`MESA`, version r22.05.1; Paxton et al. 2011, 2013, 2015, 2018, 2019) to trace the detailed evolution of binary systems in the hybrid CONe WD + MS channel. We start our binary evolution calculations when a CONe WD + MS binary system is formed. In our calculations, the detailed structures of MS companion stars is resolved consistently, and the CONe WD is treated as a point mass. The metallicity is set to be $Z = 0.0001$. This is the lowest metallicity that our codes are able to calculate. We therefore simply take $Z = 0.0001$ as an extreme case to investigate SN Ia rates and their delay times in metal-poor environments (see also Meng et al. 2009; Chen et al. 2019). We assume that the MS star transfers hydrogen-rich (H-rich) material to the WD through the Roche-lobe overflow (RLOF). If the WD grows in mass to reach the near-Chandrasekhar-mass limit (which is assumed to be $1.378\,M_{\odot}$ in this work), we assume that it would explode as an SN Ia (Nomoto et al. 1984). We set the ratio of typical mixing length to the local pressure scaleheight, $\alpha = l/H_p$, to 2. In addition, the convective overshooting parameter, $\delta_{\rm ov}$, is set to 0.12 (Pols et al. 1997; Schroder et al. 1997), which means that the overshooting length is approximately equal to 0.25 pressure scaleheights (H_p).

In this work, we focus on the hybrid CONe WD+MS channel for SNe Ia. In Chen et al. (2014), they suggest that a hybrid CONe WD forms when a massive AGB star stalls its CO core burning due to the convective boundary mixing. They further showed that the formed CONe WDs have a range of masses of 1.02–1.30 $M_{\odot}$ for a range of CBR factors of 0.1–10. Following the results of Chen et al. (2014), we therefore set a mass range of our initial CONe WDs to 1.0–1.3 $M_{\odot}$ in our detailed binary evolution calculations. It is important to note that the CBR during the C-burning process is quite uncertain. For instance, taking the possible resonance and hindrance effects (Jiang et al. 2007; Spillane et al. 2007) into account could cause the values of the CBR to change by a few orders of magnitude (Chen et al. 2014). Therefore, we treat the CBR as a free parameter in our calculations and set it to be the same values as used in Chen et al. (2014).

As the MS companion star evolves, it expands to fill its Roche lobe during either the MS phase or the Hertzsprung gap (HG) phase. As a result, the companion star starts to transfer H-rich material to the WD through RLOF. As described in Han & Podsiadlowski (2004), we also adopt the prescription of Hachisu et al. (1999) for the accumulation of transferred H-rich material onto the CONe WD (i.e., the mass growth of a CONe WD). If the mass-transfer rate ($|\dot{M}_2|$) is above the critical rate ($\dot{M}_{\rm cr}$), we assume that the transferred H burns steadily on the surface of WD and that the accreted H-rich material converts into He at a rate of $\dot{M}_{\rm cr}$, and the unprocessed H-rich material will lose from the binary system in optically thick wind. Here, the critical mass-transfer rate is given as follows (see also Hachisu et al. 1999).

$$\dot{M}_{\rm cr} = 5.3 \times 10^{-7}\frac{(1.7 - X)}{X}(M_{\rm WD} - 0.4), \quad (1)$$

where $M_{\rm WD}$ is the mass of the accreting WD (mass is in $M_{\odot}$) and X is the H mass fraction.

If $|\dot{M}_2|$ is lower than $\dot{M}_{\rm cr}$, different assumptions are adopted for the mass growth of the accreting WD: (i) when $|\dot{M}_2|$ is higher than $\frac{1}{8}\dot{M}_{\rm cr}$, we assume that the transferred H-rich material will burn steadily on the WD surface or that the weak H flashes occur, and all the transferred material would retain onto the WD. (ii) When the $|\dot{M}_2|$ is lower than $\frac{1}{8}\dot{M}_{\rm cr}$, H-shell flashes are too strong to accumulate any transferred material. Therefore, the accumulation rate of the He-shell of the accreting WD can be described as follows.

$$\dot{M}_{\rm He} = \eta_{\rm H}|\dot{M}_2|, \quad (2)$$

where

$$\eta_{\rm H} = \begin{cases} \dot{M}_{\rm cr}/|\dot{M}_2|, & |\dot{M}_2| > \dot{M}_{\rm cr}, \\ 1, & \dot{M}_{\rm cr} \geqslant |\dot{M}_2| \geqslant \frac{1}{8}\dot{M}_{\rm cr}, \\ 0, & |\dot{M}_2| < \frac{1}{8}\dot{M}_{\rm cr}. \end{cases} \quad (3)$$

We further assume that the He ignites when the He layer reaches a certain mass and that He is converted into CO. The He flashes may occur during the He-shell burning and a portion of the shell mass is assumed to be blown away in our calculations. In this work, the mass accumulation efficiency for He-shell flashes is taken from Hachisu et al. (1999), which can

be described as follows.

$$\eta_{\rm He} = \begin{cases} -0.175(\log_{10}\dot{M}_{\rm He} + 5.35)^2 + 1.05, \\ \qquad\qquad -7.3 < \log_{10}\dot{M}_{\rm He} < -5.9, \\ 1, \qquad\qquad -5.9 \leqslant \log_{10}\dot{M}_{\rm He} \leqslant -5, \end{cases} \quad (4)$$

Finally, we can calculate the mass growth rate (i.e., $\dot{M}_{\rm WD}$) of an accreting CONe WD, which is

$$\dot{M}_{\rm WD} = \eta_{\rm He}\dot{M}_{\rm CO} = \eta_{\rm He}\eta_{\rm H}|\dot{M}_2|. \quad (5)$$

The mass lost from the binary system is assumed to take away the specific orbital angular momentum of the accreting WD. According to the results of Chen et al. (2014, see their Figure 5), we consider the cases with different CBR factors of 0.1, 1.0 and 10.0, and set the initial mass of CONe WD ($M^i_{\rm WD}$) ranges from 1.0 to 1.3 $M_\odot$. For the WDs with a mass range of 1.0–1.2 $M_\odot$, we set the initial mass range of the donor star (M^i_2) to 1.0−3.6 $M_\odot$, which is consistent with that in Meng & Podsiadlowski (2014). For the cases with a WD mass of 1.3 $M_\odot$, we range the donor mass M^i_2 from 1.0 $M_\odot$ to 4.0 $M_\odot$. In addition, we set a range of initial orbital periods (P_i) to 0.25–20 days.

2.2. Binary Population Synthesis

In order to calculate the birth rates and delay times of SNe Ia produced from the CONe WD + MS channel, we perform a series of population synthesis calculations with the rapid binary evolution code developed by Hurley et al. (2000, 2002), i.e., the `Binary Star Evolution (BSE)` code. The `BSE` code can evolve a large number of binary systems rapidly from ZAMS to the formations of CONe WD + MS binary systems. The basic assumptions and treatments for some fundamental processes in our population synthesis calculations are similar to those in Meng & Podsiadlowski (2014), which are briefly described as follows.

2.2.1. Formation of CONe WD + MS Systems

In Figure 5 of Chen et al. (2014), they have provided mass boundaries that allow to form CO WDs, ONe WDs and hybrid CONe WDs for different CBR factors. Usually, CO cores in the AGB stars with significantly large masses will go through a C-burning process and evolve into an ONe core. However, according to Denissenkov et al. (2013), the C-burning process may stall due to the convective boundary mixing and form a hybrid CONe core. Since the convective boundary mixing process is not considered in the `BSE` code, hybrid CONe WDs will be mis-evaluated into ONe WDs in our rapid binary evolution calculations. We therefore simply assume that a WD would be a hybrid CONe WD if its mass is lower than the upper-limit mass boundaries of hybrid CONe WDs given by Figure 5 of Chen et al. (2014, the upper-panel) and appear to be a ONe WD in the binary population synthesis (see also Meng & Podsiadlowski 2014).

Based on the results of Chen et al. (2014), we performed BPS calculations for three different CBR factors of 0.1, 1 and 10. If a CONe WD + MS binary system is formed and its binary parameters at the onset of RLOF fall into the initial contours in $\log_{10}P^i$ –M^i_2 plane given by our detailed binary evolution calculation in Section 2.1, we assume that this system would eventually explode as an SN Ia.

2.2.2. Treatment for Common-envelope Evolution

Different binary systems start their first RLOF in different stages, which depend on the mass, mass ratios and orbital periods. Whether or not a binary system can lead to dynamically unstable mass-transfer to form a CE mainly depends on the mass ratio of the system at the onset of RLOF. If the mass ratio is larger than the critical mass ratio, q_c, the dynamically unstable RLOF will happen to form a CE. Here, the critical ratio q_c varies with the evolutionary stages of the binary systems at the onset of RLOF (Hjellming & Webbink 1987; Webbink 1988; Han et al. 2002; Podsiadlowski et al. 2002; Chen & Han 2008). Based on the results of previous detailed binary evolution studies (e.g., Han et al. 2000; Chen & Han 2002, 2003), we set $q_c = 4.0$ when the primary star is either on the MS phase or on the HG phase. If the primary star is a naked He giant, we set $q_c = 0.748$. If the primary star is on the first giant branch or AGB, we set q_c as follows.

$$q_c = \left[1.67 - x + 2\left(\frac{M^{\rm P}_{\rm c1}}{M^{\rm P}_1}\right)\right] \Big/ 2.13 \quad (6)$$

The filled circles and cross symbols respectively indicate that the binary systems that can and cannot successfully lead to SNe Ia. Here M^P_1 and $M^P_{\rm c1}$ are the mass and the core mass of the primary star, respectively; $x = d\ln R^P_1/d\ln M^P_1$ is the mass–radius exponent of the primary star, which varies with composition.

Binary systems inside the CE are expected to release their orbital energies through the frictional drag and then undergo an in-spiral. The released energy would be partly used to eject the CE. Once a binary system enters the CE phase, we assume that the CE could be ejected completely if

$$\alpha_{\rm CE}\Delta E_{\rm orb} = |E_{\rm bind}|, \quad (7)$$

where $\Delta E_{\rm orb}$ is the orbital energy released during the spiral-in phase, $E_{\rm bind}$ is the binding energy of the CE, and $\alpha_{\rm CE}$ is the CE ejection efficiency. Because the internal energy in the CE is not incorporated into the binding energy, $\alpha_{\rm CE}$ may be greater than 1. The exact value of $\alpha_{\rm CE}$ is still poorly constrained from both theoretical and observational sides (e.g., Zorotovic et al. 2010; Ivanova et al. 2013; Toonen & Nelemans 2013; Röpke & De Marco 2023; Scherbak & Fuller 2023; Ge et al. 2024). In this

work, similar to various previous works (e.g., Meng et al. 2009; Meng & Podsiadlowski 2014, 2018; Liu & Stancliffe 2018; Wang et al. 2013, 2014, 2017), we simply set $\alpha_{\rm CE}$ to be 0.5, 0.75, 1.0 and 3.0, to investigate the influence of different CE ejection efficiencies on the results. $E_{\rm bind}$ is given by

$$E_{\rm bind} = \frac{GM_{\rm 1}^{\rm P}{\rm M}_{\rm e1}^{P}}{\lambda_{\rm CE}\, R_{\rm 1}^{\rm P}}, \quad (8)$$

Where G is the gravitational constant, and $M_{c1}^{\rm P}$ is the mass of the removed envelope from the giant primary. Here $M_{\rm e1}^{\rm P} = M_{\rm 1}^{\rm P} - M_{\rm c1}^{\rm P}$. $R_{\rm 1}^{\rm P}$ is the radius of the primary giant star at the onset of CE, while $\lambda_{\rm CE}$ is the binding energy factor, which is set to characterize the envelope central concentration of the giant primary. In this work, the binding energy factor is set to be $\lambda_{\rm CE} = 0.5$.

2.2.3. Basic Assumptions

We use a Monte Carlo method to generate a large number of binary systems and follow their rapid evolution from the ZAMS phase to the formation of CONe WD + MS systems. The basic assumptions adopted in our rapid calculations are described as follows:

(1) We assume that all stars are in binary systems. Also, all binary systems are assumed to have a circular orbit.

(2) We use the initial mass function (IMF) given by Miller & Scalo (1979). The primary star is generated according to the formula of Eggleton et al. (1989):

$$M_{\rm 1}^{P} = \frac{0.19 \quad R}{(1-R)^{0.75} + 0.0032(1-R)^{0.25}}, \quad (9)$$

where R is a random number uniformly distributed in the range [0,1], $M_{\rm 1}^{P}$ is the mass of the primary star, which is between $0.1\,M_{\odot}$ and $100\,M_{\odot}$.

(3) We assume that the mass ratios of the initial binary systems at the ZAMS phase, q', have a constant distribution (Mazeh et al. 1992; Goldberg & Mazeh 1994).

$$n(q') = 1, \quad 0 < q' \leqslant 1, \quad (10)$$

where $q' = M_{\rm 1}^{P}/M_{\rm 2}^{P}$.

(4) We assume that the distribution of binary separations is constant in $\log a$ for wide binary systems(where a is separation), and falls off smoothly for close binary systems (Han et al. 1995):

$$a \cdot n(a) = \begin{cases} \alpha_{\rm sep}(a/a_0)^{\rm m} & a \leqslant a_0, \\ \alpha_{\rm sep}, & a_0 < a < a_1, \end{cases} \quad (11)$$

where $\alpha_{\rm sep} \approx 0.07$, $a_0 = 10\,R_{\odot}$, $a_1 = 5.75 \times 10^6\,R_{\odot} = 0.13$ pc and $m \approx 1.2$. This distribution implies that the number of wide binary systems per logarithmic interval is equal and about 50% of binary systems have orbital periods less than 100 yr (Han et al. 1995).

(5) Either a single starburst with $10^{11}\,M_{\odot}$ or a constant star formation rate (SFR) of $5\,M_{\odot}\,{\rm yr}^{-1}$ in the past 15 Gyr is assumed in our calculations.

3. Results

In this section, we present the main results from our detailed binary evolution and population synthesis calculations, including the initial parameter spaces (i.e., the orbital period-secondary mass plane; $\log_{10} P^{i} - M_{2}^{i}$) which eventually lead to SNe Ia in the hybrid CONe WD + MS channel, and the predicted birth rates and delay times of SNe Ia from this channel.

3.1. Initial Parameter Contours

We use the MESA code to perform detailed binary evolution calculations for about 1000 binary systems consisting of a CONe WD (which is treated as a point mass) and an MS companion star by using the method described in Section 2.1. The initial masses of CONe WDs and MS companions and orbital periods of these binary systems cover the ranges of $1.0\,M_{\odot} \leqslant M_{\rm WD}^{i} \leqslant 1.3\,M_{\odot}$, $1.0\,M_{\odot} \leqslant M_{2}^{i} \leqslant 4.0\,M_{\odot}$ and $-0.6 \leqslant \log_{10} P^{i} \leqslant 1.3$, respectively. Figure 1 presents the results from our detailed binary evolution calculations in the $\log_{10} P^{i} - M_{2}^{i}$ plane for different given initial WD masses. The filled circles and cross symbols in Figure 1 respectively correspond to the models that are able and unable to successfully produce SN Ia explosions in our calculations. *The left boundaries* of initial contours (solid lines) in Figure 1 are constrained by the requirement that the binary systems do not fill their Roche lobes before the MS phase. Binary systems outside *the upper boundaries* of the contours subsequently experience dynamically unstable mass-transfer and lead to CE objects. For binary systems outside *the right boundaries*, their mass-transfer rates are too high to lead to a long enough mass-transfer phase. This inhibits the WDs from accumulating mass to reach the Chandrasekhar limit.[7] For binary systems below *the lower boundaries* of the contours, the MS donors are not massive enough to lead to sufficient mass-transfer rates to allow the WDs to accumulate mass to reach the Chandrasekhar limit.

As shown in Figure 1, the contours for the initial CONe WD mass of $1.3\,M_{\odot}$ extend to a significantly higher initial donor mass (the upper boundary) compared to those of other models, i.e., the enclosed region of this contour is much larger. This is because the binary systems close to the upper boundaries may go through a short dynamically stable mass-transfer phase before the dynamically unstable mass-transfer starts. This phase will only allow a small amount of mass accumulation

[7] Note that a small number of systems with a high initial WD mass ($M_{\rm WD}^{i} \geqslant 1.1\,M_{\odot}$) and a low initial MS mass ($M_{2}^{i} \leqslant 2.0\,M_{\odot}$) outside the right boundaries can still undergo dynamically stable mass-transfer when the donor star evolves to the base of red giant branch (RGB) to eventually lead to SNe Ia. In this work, however, we only focus on the hybrid CONe WD + MS channel.

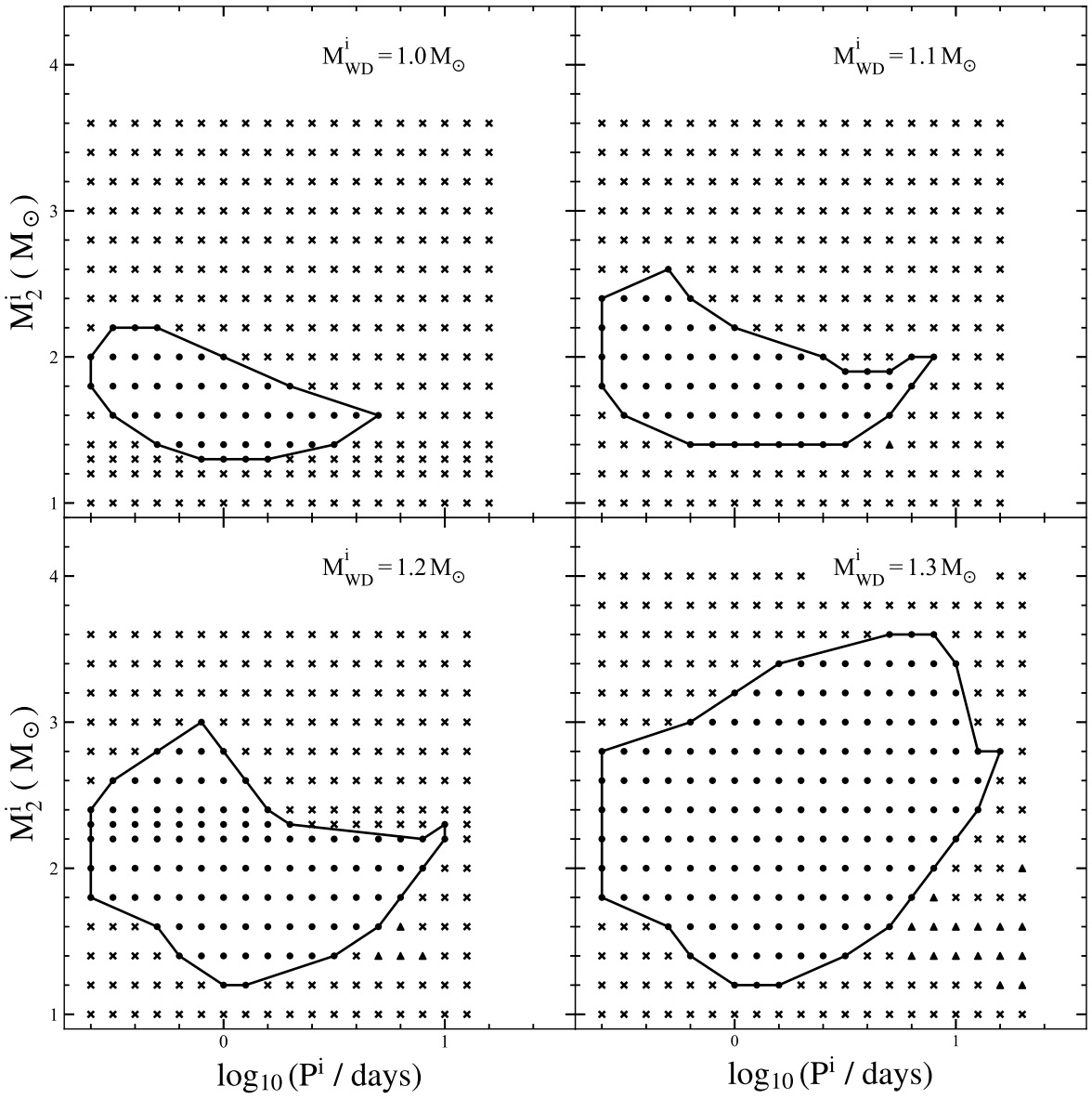

Figure 1. Results in the orbital period–secondary mass ($\log_{10} P^i - M_2^i$) plane for the CONe WD + MS channel at $Z = 0.0001$ from our detailed binary evolution calculations. Here, P^i and M_2^i are the initial orbital period and companion mass, respectively. The filled circles and cross symbols respectively indicate the binary systems that can and cannot successfully lead to SNe Ia. Different panels correspond to the results with different initial CONe WD masses ($M^i_{\rm WD}$).

(~0.1 $M_\odot$) onto the CONe WD due to the short timescale. Thus, only a 1.3 $M_\odot$ CONe WD can accumulate enough mass to reach a mass of 1.378 $M_\odot$ to trigger an SN Ia explosion.

3.2. Results of Binary Population Synthesis

By using the method described in Section 2.2, we follow a rapid evolution of 10^8 binary systems from the ZAMS phase to the formation of CONe WD + MS systems. Once the formed CONe WD + MS systems fall into the initial contours given by detailed binary evolution calculations(i.e., Figure 1) at the moment of RLOF, we simply assume that the systems would eventually lead to successful SN Ia explosions. In Figure 2, we present the predicted birth rates of SNe Ia from our BPS calculations for the hybrid CONe WD + MS channel by assuming a constant star formation rate (SFR) of ~5 $M_\odot\,{\rm yr}^{-1}$ over the past 15 Gyr. As shown in Figure 2, the SN Ia rate in a galaxy with a constant SFR is affected not only by the assumed CE ejection efficiencies in our BPS calculations but also by the adopted CBR factors. Depending on different $\alpha_{\rm CE}$ and CBR factors, we find that the SN Ia rate in a galaxy with a constant

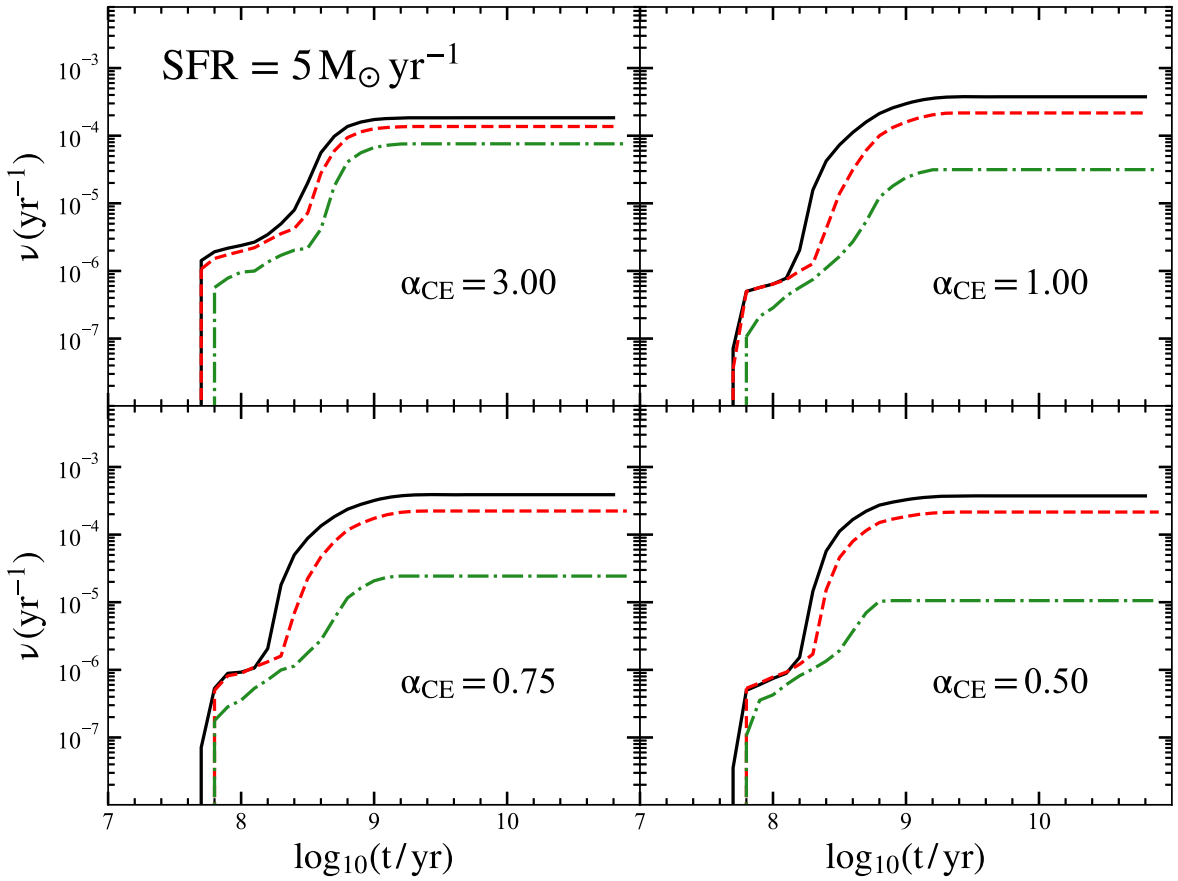

Figure 2. Evolution of SN Ia birth rates from the CONe WD + MS channel for a constant star formation rate of SFR = 5 $M_{\odot}$ yr^{-1}. The results with different CE ejection efficiencies ($\alpha_{\rm CE}$ = 0.50, 0.75, 1.00 and 3.00) are indicated in each panel. The solid, dashed and dashed–dotted lines represent the cases for CBR factors of 0.1, 1, and 10 (Chen et al. 2014), respectively.

SFR in the hybrid CONe WD + MS channel at $Z = 0.0001$ is about 0.11–3.89 $\times$ 10^{-4} yr^{-1}. In addition, Figure 2 shows that a lower $\alpha_{\rm CE}$ tends to give a higher SN Ia rate. This is because the lower the $\alpha_{\rm CE}$ values are, the more orbital energy will be lost when the primordial binary systems eject the CE to form a CONe WD + MS system. As a result, the CONe WD + MS systems will have shorter initial orbital separations. This refers to a shorter initial Roche-lobe radius, thus more easily to start the RLOF, leading to higher SN Ia rates.

Figure 3 presents the delay-time distributions (DTDs) of SNe Ia in the hybrid CONe WD + MS channel at $Z = 0.0001$ after a starburst of $10^{11} M_{\odot}$. We find that the delay times of SNe Ia in this channel cover a range of 0.05–2.5 Gyr. Two peaks are observed in the DTDs of SNe Ia, which is in consistent with the result shown in Meng & Podsiadlowski (2014). The right peak, around 0.3 Gyr, is given by SNe Ia produced from normal CONe WD + MS evolutionary channel. The left peak, around 0.06 Gyr, is from the so-called He-enriched MS (HEMS) evolutionary channel (see Meng et al. 2009; Liu & Stancliffe 2018, for a detailed description). In the HEMS channel, the primary star begins its first episode of RLOF mass-transfer during the HG phase or during the RG phase. The binary system then undergoes a CE phase due to the dynamically unstable mass-transfer. After the CE ejection, the primary He star and a companion MS star remained in the system. As the primary He star continues to evolve and expand, the second episode of RLOF mass-transfer occurs. In this phase, He-rich material transfers onto the surface of the companion MS star and eventually forms a CONe WD + HEMS binary system (Liu & Stancliffe 2018). SNe Ia formed in the hybrid CONe WD + HEMS channel have relatively shorter delay times compared to those of the normal hybrid CONe WD + MS channel.

Figure 4 shows the mass distribution of the initial hybrid CONe WDs of the systems which successfully produce SNe Ia. The lower- and upper-limits for the initial CONe WD masses (which are about 1.02 $M_{\odot}$ and 1.30 $M_{\odot}$) are respectively constrained by the upper-limits for CO WD and CONe WD masses given by Figure 5 of Chen et al. (2014). The difference in distribution between the CBR factor of 0.1 and 1 is relatively small, leading to that the SN Ia rates of these two cases are

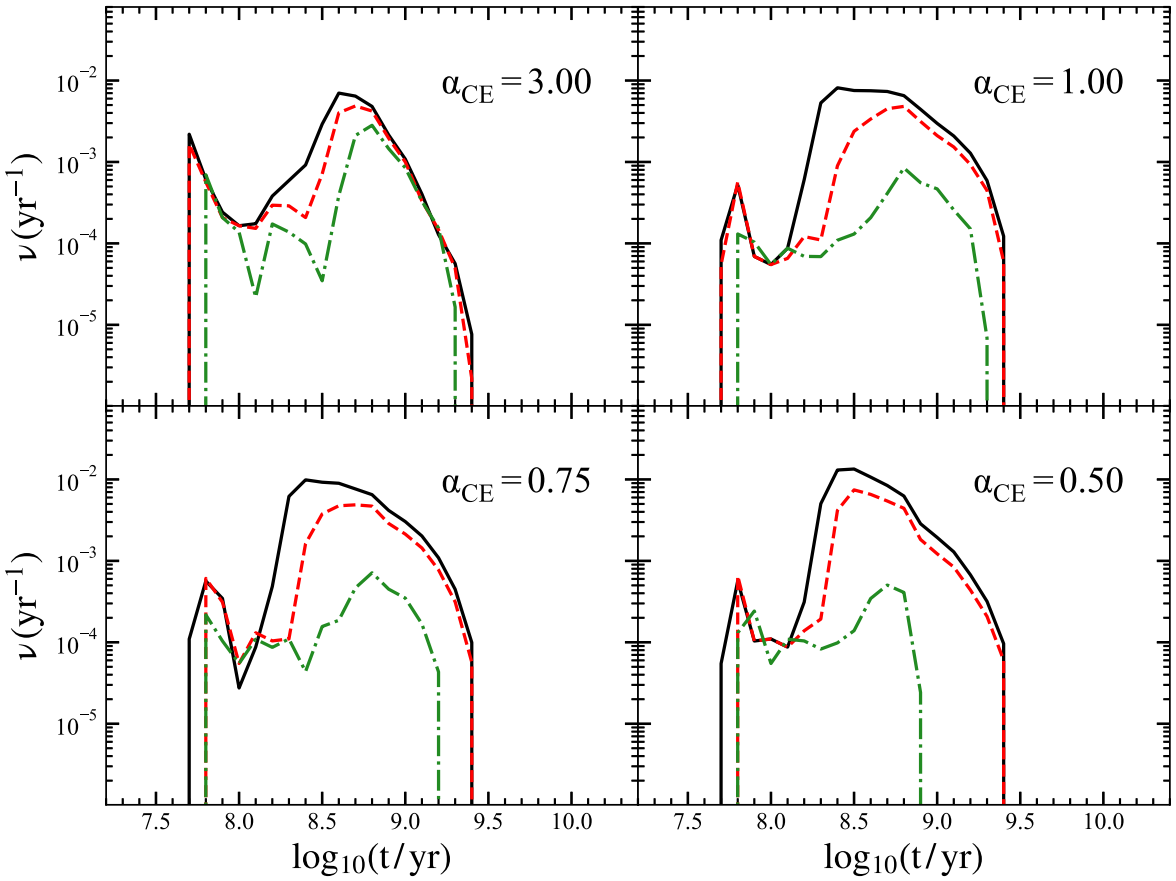

Figure 3. Similar to Figure 2, but for a single starburst of $10^{11}\,M_{\odot}$.

quite similar (see Figures 2 and 3). For a CBR factor of 10, however, more CONe WD + MS systems that fulfill the condition for SN Ia production are formed as the α_{CE} factors increase, as well as the SN Ia rates shown in Figure 2.

4. Discussion

4.1. Comparisons with Previous Works

In Figure 5, we compare the initial contours in the $\log_{10} P^i - M_2^i$ plane from our detailed binary evolution calculations ($Z = 0.0001$) to those given by previous work of Meng & Podsiadlowski (2014) with $Z = 0.02$. It shows that our contours cover shorter orbital periods and lower MS companion masses than theirs. Similar trends are also shown in the binary systems from the CO WD + MS channel in Meng et al. (2009). In Figure 6, we further compare the predicted SNe Ia rates in a galaxy with a constant SFR and delay times of SNe Ia between two metallicities. Here, only the results with a CBR factor of 0.1 are presented. It shows that the SNe Ia rates in a galaxy with a constant SFR do not change significantly as the metallicity varies from $Z = 0.02$ to $Z = 0.0001$. However, Figure 6 shows that SNe Ia have relatively longer delay times in lower-metallicity environments. This is because progenitor systems in lower-metallicity environments have smaller initial secondary masses (see Figure 5), leading to longer evolutionary timescales until they fill their Roche lobe and thus longer delay times (see also Meng et al. 2009).

To compare our results with the observations, following the previous work of Kistler et al. (2013), we simply calculate the galactic masses in a low metallicity galaxy with $Z = 0.0001$ by using the relation between stellar metallicities and galactic masses derived from Sloan Digital Sky Survey (SDSS) observations (Gallazzi et al. 2005). This gives a galactic mass of $\sim 2.5 \times 10^7\,M_{\odot}$ for $Z = 0.0001$. We then the observational relation between SNe Ia birth rates and stellar masses provided by Wiseman et al. (2021) to calculate the expected SN Ia rates at $Z = 0.0001$, which is $\sim 6.6 \times 10^{-5}\,\mathrm{yr}^{-1}$. These rates are relatively lower than those from our BPS calculations of $\sim 3.9 \times 10^{-4}\,\mathrm{yr}^{-1}$ by a factor of 6. However, it is important to note that BPS calculations have some uncertainties (e.g., Han et al. 2020, see also Section 4.2). Also, we directly use the relations given by Gallazzi et al. (2005) and Wiseman et al. (2021)

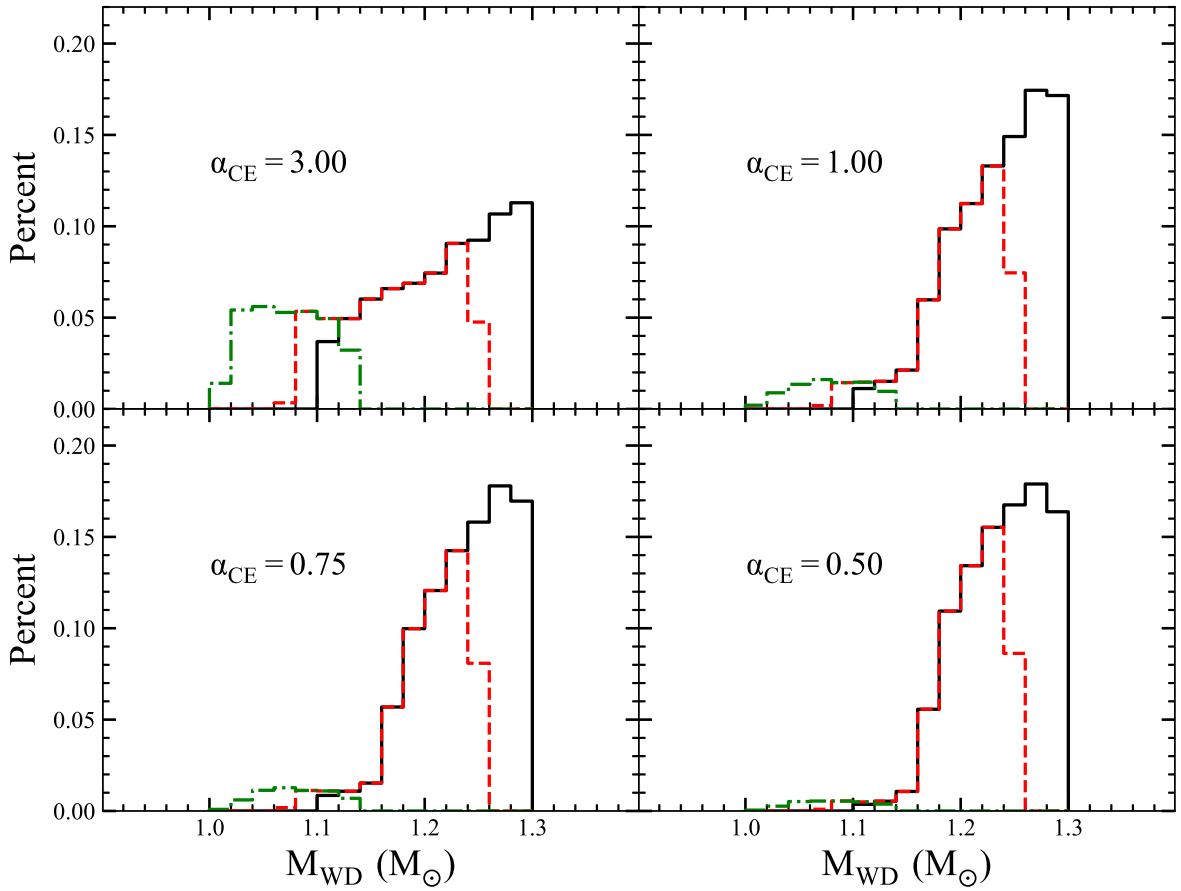

Figure 4. Distributions of the initial masses of hybrid CONe WDs from our population synthesis calculations with different CBR factors and CE ejection efficiencies (α_{CE}). Different lines indicate the same CBR factors as in Figures 2 and 3.

for calculations under some assumptions such as that the effect of redshift could be neglected. This may lead to some uncertainties on the expected SN Ia rates at $Z = 0.0001$.

4.2. Uncertainties of Our Results

In this work, we simply assume that all stars are in binary systems. This means that our calculations only present upper-limits of the SNe Ia birth rates. We also assume that all the binary systems are in circular orbits. This assumption may lead to some uncertainties in the results. In previous work of Wang et al. (2013), they investigated the effect of different initial eccentricities on their BPS results. They suggested that different initial eccentricities lead to a small difference in rates and delay times of SNe Ia from their BPS calculations compared with those with an assumption of a circular orbit. In addition, we simply use a constant SFR of $\sim 5\,M_\odot$ for our calculations, which could lead to SN Ia rates in Figure 6 are under-or over-estimated. For comparison, we adopt a variable SFR given by Kubryk et al. (2015) to study its effect on SN Ia rates. As shown in Figure 6, with a variable SFR, SN Ia rates rise and reach a peak at delay times around 1 Gyr, then decline exponentially. This indicates that different SFRs are needed to be taken into account in BPS studies for SNe Ia.

We adopt the optically thick wind model (Hachisu et al. 1996, 1999; Kato & Hachisu 1999) for the treatment of the mass accumulation efficiency onto the WDs. However, the exact mass accumulation efficiency is still not well-constrained, which might bring some uncertainties on our results. Previous BPS studies have shown that adopting different mass accumulation efficiencies onto the WDs in BPS calculations could give a significant difference in the predicted SN Ia rates (e.g., Piersanti et al. 2014; Ruiter et al. 2014; Toonen et al. 2014).

We have tested the influence of different CE ejection efficiencies on the results by varying the values of α_{CE} from 0.5 to 3.0 in our BPS calculations. However, current constraints on the CE ejection efficiency are still quite weak. Meanwhile, a fixed binding energy factor value ($\lambda_{CE} = 0.5$) is used for all evolutionary phases in a single BPS calculations (see also Meng & Podsiadlowski 2014). Ivanova (2011) suggested that the value of λ_{CE} is dependent on the relative mass distribution

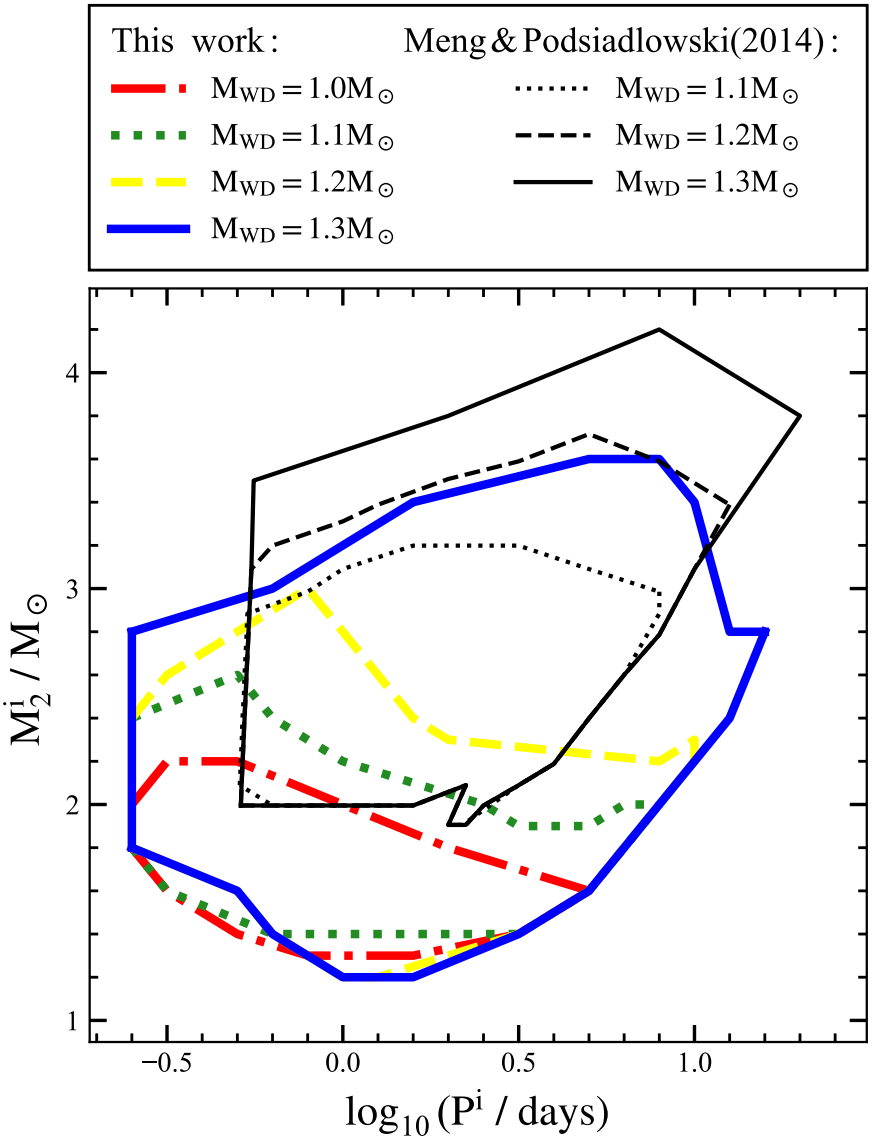

Figure 5. Comparison of initial parameter spaces between our work (*thick color lines*) and the previous study of Meng & Podsiadlowski (2014) with $Z = 0.02$ (*thin black lines*). Results with different initial CONe WD masses are indicated by different line-styles.

of the envelope of the donor stars, thus leading to that the exact λ_{CE} value might vary with different evolutionary phases. In addition, other initial conditions and assumptions in BPS calculations such as the SFR and initial mass function are still quite uncertain (see Claeys et al. 2014, for a detailed description of theoretical uncertainties in BPS studies of SNe Ia). This may also lead to some uncertainties in our BPS results.

5. Summary

In this work, we have addressed the rates and delay times of SNe Ia produced from the hybrid CONe WD + MS channel at low metallicity of $Z = 0.0001$ by combining the results of detailed binary evolution calculation with MESA (Paxton et al. 2011, 2013, 2015, 2018, 2019) into the population synthesis models computed from BSE (Hurley et al. 2000, 2002). We adopt the 'optically thick wind model' for the treatment of the mass accumulation efficiency onto the accreting CONe WD. Compared with previous works for solar-like metallicity of $Z = 0.02$ (Meng & Podsiadlowski 2014), we attempt to explore how different metallicities affect the rates and delay times of SNe Ia in the hybrid CONe WD + MS channel. Our main results and conclusions can be summarized as follows.

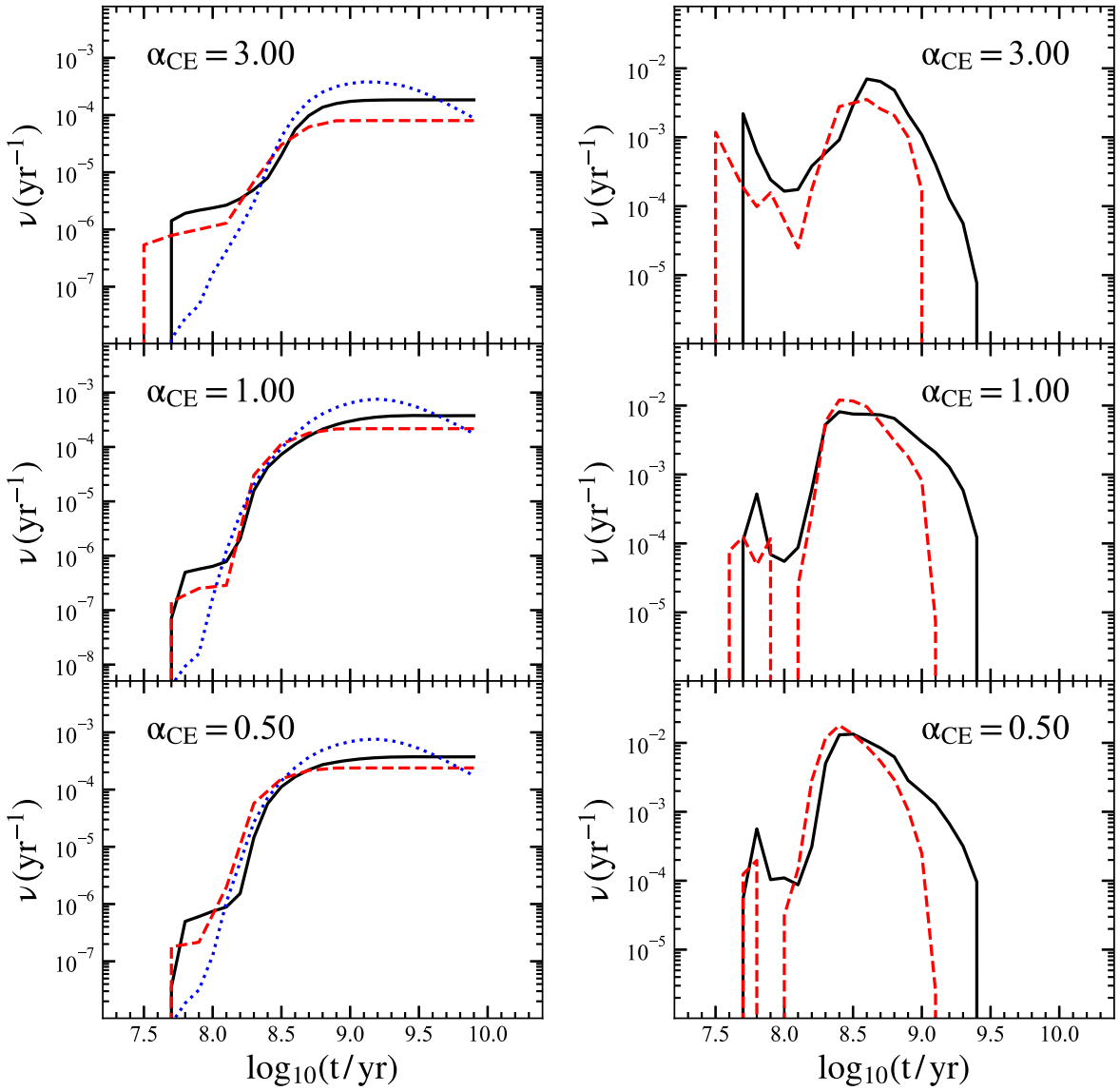

Figure 6. Comparison of birth rates and delay times of SNe Ia in a galaxy with a constant SFR (left panels) and in a starburst galaxy (right panels). Black solid lines are the results from this work with a constant SFR model, blue dotted lines are the results from this work with a variable SFR model adopted from Kubryk et al. (2015) and red dashed lines are the results from the previous work of Meng & Podsiadlowski (2014) with $Z = 0.02$. Here, only the results with a CBR factor of 0.1 are given for comparison.

(1) Depending on different CE ejection efficiencies and CBR factors adopted in BPS calculations, we find that the SN Ia rates in a galaxy with a constant SFR of ~5 $M_\odot$ from the hybrid CONe WD + MS channel at low metallicity of $Z = 0.0001$ are $(0.11-3.89) \times 10^{-4}\,\mathrm{yr}^{-1}$.

(2) The DTDs of SNe Ia from the hybrid CONe WD + MS channel at $Z = 0.0001$ cover a wide range of 0.05–2.5 Gyr, and most SNe Ia have delay times of 0.3 Gyr.

(3) Comparing with previous works of Meng & Podsiadlowski (2014) for $Z = 0.02$, we find that SN Ia rates and delay times given by our work are not significantly different from theirs, although SNe Ia produced at low metallicity environment of $Z = 0.0001$ have relatively longer delay times.

Acknowledgments

We are grateful to Hai-Liang Chen, Zhenwei Li, Yunlang Guo and Lifu Zhang for their fruitful discussions. This work is supported by the Strategic Priority Research Program of the Chinese Academy of Sciences (grant Nos. XDB1160303, XDB1160000), the National Natural Science Foundation of China (NSFC, Nos. 12288102, 12333008, 12090040/1, 11873016, 11973080, and 11803030), the National Key R&D Program of China (Nos. 2021YFA1600403, 2021YFA1600401 and 2021YFA1600400), the Chinese Academy of Sciences (CAS), the Yunnan Ten Thousand Talents Plan–Young & Elite Talents Project, and the CAS "Light of West China" Program, the International Centre of Supernovae, Yunnan Key Laboratory (No. 202302AN360001), the Yunnan Fundamental Research Projects (grant Nos. 202401BC070007, 202201BC070003, and 202001AW070007) and the "Yunnan Revitalization Talent Support Program"—Science & Technology Champion Project and Yunling Scholar Project (No. 202305AB350003).

References

Antoniadis, J., Chanlaridis, S., Gräfener, G., & Langer, N. 2020, A&A, 635, A72
Bauer, E. B., White, C. J., & Bildsten, L. 2019, ApJ, 887, 68
Bedin, L. R., Ruiz-Lapuente, P., González Hernández, J. I., et al. 2014, MNRAS, 439, 354
Bloom, J. S., Kasen, D., Shen, K. J., et al. 2012, ApJL, 744, L17
Boehner, P., Plewa, T., & Langer, N. 2017, MNRAS, 465, 2060
Chen, H.-L., Woods, T. E., Yungelson, L. R., et al. 2019, MNRAS, 490, 1678
Chen, M. C., Herwig, F., Denissenkov, P. A., & Paxton, B. 2014, MNRAS, 440, 1274
Chen, X., & Han, Z. 2002, MNRAS, 335, 948
Chen, X., & Han, Z. 2003, MNRAS, 341, 662
Chen, X., & Han, Z. 2008, MNRAS, 387, 1416
Claeys, J. S. W., Pols, O. R., Izzard, R. G., Vink, J., & Verbunt, F. W. M. 2014, A&A, 563, A83
Denissenkov, P. A., Herwig, F., Truran, J. W., & Paxton, B. 2013, ApJ, 772, 37
Denissenkov, P. A., Truran, J. W., Herwig, F., et al. 2015, MNRAS, 447, 2696
Dilday, B., Howell, D. A., Cenko, S. B., et al. 2012, Sci, 337, 942
Dimitriadis, G., Foley, R. J., Rest, A., et al. 2019, ApJL, 870, L1
Dimitriadis, G., Sullivan, M., Kerzendorf, W., et al. 2017, MNRAS, 468, 3798
Eggleton, P. P., Fitchett, M. J., & Tout, C. A. 1989, ApJ, 347, 998
Elias-Rosa, N., Chen, P., Benetti, S., et al. 2021, A&A, 652, A115
Fink, M., Kromer, M., Seitenzahl, I. R., et al. 2014, MNRAS, 438, 1762
Foley, R. J., Challis, P. J., Chornock, R., et al. 2013, ApJ, 767, 57
Fuhrmann, K. 2005, MNRAS, 359, L35
Fujimoto, M. Y. 1982a, ApJ, 257, 752
Fujimoto, M. Y. 1982b, ApJ, 257, 767
Gallazzi, A., Charlot, S., Brinchmann, J., White, S. D. M., & Tremonti, C. A. 2005, MNRAS, 362, 41
Garcìa-Berro, E., Ritossa, C., & Iben, I. J. 1997, ApJ, 485, 765
Ge, H., Tout, C. A., Webbink, R. F., et al. 2024, ApJ, 961, 202
Geier, S., Fürst, F., Ziegerer, E., et al. 2015, Sci, 347, 1126
Goldberg, D., & Mazeh, T. 1994, A&A, 282, 801
González Hernández, J. I., Ruiz-Lapuente, P., Filippenko, A. V., et al. 2009, ApJ, 691, 1
Graham, M. L., Kumar, S., Hosseinzadeh, G., et al. 2017, MNRAS, 472, 3437
Graham, M. L., Nugent, P. E., Sullivan, M., et al. 2015, MNRAS, 454, 1948
Hachisu, I., Kato, M., & Nomoto, K. 1996, ApJL, 470, L97
Hachisu, I., Kato, M., Nomoto, K., & Umeda, H. 1999, ApJ, 519, 314
Hamers, A. S., Pols, O. R., Claeys, J. S. W., & Nelemans, G. 2013, MNRAS, 430, 2262
Han, Z., & Podsiadlowski, P. 2004, MNRAS, 350, 1301
Han, Z., Podsiadlowski, P., & Eggleton, P. P. 1995, MNRAS, 272, 800
Han, Z., Podsiadlowski, P., Maxted, P. F. L., Marsh, T. R., & Ivanova, N. 2002, MNRAS, 336, 449
Han, Z., Tout, C. A., & Eggleton, P. P. 2000, MNRAS, 319, 215
Han, Z.-W., Ge, H.-W., Chen, X.-F., & Chen, H.-L. 2020, RAA, 20, 161
Hayden, B., Rubin, D., Boone, K., et al. 2021, ApJ, 912, 87
Hjellming, M. S., & Webbink, R. F. 1987, ApJ, 318, 794
Holmbo, S., Stritzinger, M. D., Shappee, B. J., et al. 2019, A&A, 627, A174
Horesh, A., Kulkarni, S. R., Fox, D. B., et al. 2012, ApJ, 746, 21
Hosseinzadeh, G., Sand, D. J., Lundqvist, P., et al. 2022, ApJL, 933, L45
Hosseinzadeh, G., Sand, D. J., Valenti, S., et al. 2017, ApJL, 845, L11
Hoyle, F., & Fowler, W. A. 1960, ApJ, 132, 565
Hurley, J. R., Pols, O. R., & Tout, C. A. 2000, MNRAS, 315, 543
Hurley, J. R., Tout, C. A., & Pols, O. R. 2002, MNRAS, 329, 897
Iben, I. J., & Renzini, A. 1983, ARA&A, 21, 271
Iben, I. J., & Tutukov, A. V. 1984, ApJS, 54, 335
Ihara, Y., Ozaki, J., Doi, M., et al. 2007, PASJ, 59, 811
Ilkov, M., & Soker, N. 2012, MNRAS, 419, 1695
Ivanova, N. 2011, in ASP Conf. Ser. 447, Evolution of Compact Binaries, ed. L. Schmidtobreick, M. R. Schreiber, & C. Tappert (San Francisco, CA: ASP), 91
Ivanova, N., Justham, S., Chen, X., et al. 2013, A&ARv, 21, 59
Jacobson-Galán, W. V., Foley, R. J., Schwab, J., et al. 2019, MNRAS, 487, 2538
Jha, S. W., Maguire, K., & Sullivan, M. 2019, NatAs, 3, 706
Jiang, C. L., Rehm, K. E., Back, B. B., & Janssens, R. V. F. 2007, PhRvC, 75, 015803
Jordan, G. C. I., Graziani, C., Fisher, R. T., et al. 2012, ApJ, 759, 53
Kashi, A., & Soker, N. 2011, MNRAS, 417, 1466
Kato, M., & Hachisu, I. 1999, ApJL, 513, L41
Katz, B., & Dong, S. 2012, arXiv:1211.4584
Kerzendorf, W. E., Schmidt, B. P., Asplund, M., et al. 2009, ApJ, 701, 1665
Kerzendorf, W. E., Yong, D., Schmidt, B. P., et al. 2013, ApJ, 774, 99
Kistler, M. D., Stanek, K. Z., Kochanek, C. S., Prieto, J. L., & Thompson, T. A. 2013, ApJ, 770, 88
Kromer, M., Fink, M., Stanishev, V., et al. 2013, MNRAS, 429, 2287
Kromer, M., Ohlmann, S. T., Pakmor, R., et al. 2015, MNRAS, 450, 3045
Kubryk, M., Prantzos, N., & Athanassoula, E. 2015, A&A, 580, A126
Lach, F., Callan, F. P., Bubeck, D., et al. 2022, A&A, 658, A179
Lattanzio, J. C., Tout, C. A., Neumerzhitckii, E. V., Karakas, A. I., & Lesaffre, P. 2017, MmSAI, 88, 248
Lecoanet, D., Schwab, J., Quataert, E., et al. 2016, ApJ, 832, 71
Leonard, D. C. 2007, ApJ, 670, 1275
Li, W., Filippenko, A. V., Chornock, R., et al. 2003, PASP, 115, 453
Liu, Z., & Stancliffe, R. J. 2020, A&A, 641, A20
Liu, Z.-W., Kromer, M., Fink, M., et al. 2013, ApJ, 778, 121
Liu, Z. W., Pakmor, R., Röpke, F. K., et al. 2012, A&A, 548, A2
Liu, Z.-W., Röpke, F. K., & Han, Z. 2023, RAA, 23, 082001
Liu, Z.-W., Röpke, F. K., Zeng, Y., & Heger, A. 2021, A&A, 654, A103
Liu, Z.-W., & Stancliffe, R. J. 2018, MNRAS, 475, 5257
Liu, Z.-W., Stancliffe, R. J., Abate, C., & Wang, B. 2015, ApJ, 808, 138
Livio, M., & Mazzali, P. 2018, PhR, 736, 1
Livio, M., Prialnik, D., & Regev, O. 1989, ApJ, 341, 299
Livio, M., & Riess, A. G. 2003, ApJL, 594, L93
Lundqvist, P., Mattila, S., Sollerman, J., et al. 2013, MNRAS, 435, 329
Lundqvist, P., Nyholm, A., Taddia, F., et al. 2015, A&A, 577, A39
Maguire, K., Taubenberger, S., Sullivan, M., & Mazzali, P. A. 2016, MNRAS, 457, 3254
Maoz, D., Mannucci, F., & Nelemans, G. 2014, ARA&A, 52, 107
Margutti, R., Parrent, J., Kamble, A., et al. 2014, ApJ, 790, 52
Marietta, E., Burrows, A., & Fryxell, B. 2000, ApJS, 128, 615
Marquardt, K. S., Sim, S. A., Ruiter, A. J., et al. 2015, A&A, 580, A118
Matteucci, F., & Greggio, L. 1986, A&A, 154, 279
Mazeh, T., Goldberg, D., Duquennoy, A., & Mayor, M. 1992, ApJ, 401, 265
McCully, C., Jha, S. W., Foley, R. J., et al. 2014, Natur, 512, 54
McCutcheon, C., Zeng, Y., Liu, Z. W., et al. 2022, MNRAS, 514, 4078
Meng, X., Chen, X., & Han, Z. 2009, MNRAS, 395, 2103

Meng, X., & Han, Z. 2016, A&A, 588, A88
Meng, X., & Podsiadlowski, P. 2014, ApJL, 789, L45
Meng, X., & Podsiadlowski, P. 2018, ApJ, 861, 127
Meng, X., & Yang, W. 2010, ApJ, 710, 1310
Miller, G. E., & Scalo, J. M. 1979, ApJS, 41, 513
Nomoto, K. 1982, ApJ, 253, 798
Nomoto, K., Saio, H., Kato, M., & Hachisu, I. 2007, ApJ, 663, 1269
Nomoto, K., Thielemann, F. K., & Yokoi, K. 1984, ApJ, 286, 644
Paczynski, B. 1976, IAU Symp. 73, Structure and Evolution of Close Binary Systems 73 ed. P. Eggleton, S. Mitton, & J. Whelan, (Cambridge: Cambridge Univ. Press), 75
Pakmor, R., Röpke, F. K., Weiss, A., & Hillebrandt, W. 2008, A&A, 489, 943
Pan, K.-C., Ricker, P. M., & Taam, R. E. 2012, ApJ, 750, 151
Patat, F., Chandra, P., Chevalier, R., et al. 2007, Sci, 317, 924
Paxton, B., Bildsten, L., Dotter, A., et al. 2011, ApJS, 192, 3
Paxton, B., Cantiello, M., Arras, P., et al. 2013, ApJS, 208, 4
Paxton, B., Marchant, P., Schwab, J., et al. 2015, ApJS, 220, 15
Paxton, B., Schwab, J., Bauer, E. B., et al. 2018, ApJS, 234, 34
Paxton, B., Smolec, R., Schwab, J., et al. 2019, ApJS, 243, 10
Perlmutter, S., Aldering, G., Goldhaber, G., et al. 1999, ApJ, 517, 565
Pierel, J. D. R., Engesser, M., Coulter, D. A., et al. 2024, ApJL, 971, L32
Piersanti, L., Tornambé, A., & Yungelson, L. R. 2014, MNRAS, 445, 3239
Podsiadlowski, P., Rappaport, S., & Pfahl, E. D. 2002, ApJ, 565, 1107
Pols, O. R., Tout, C. A., Schroder, K.-P., Eggleton, P. P., & Manners, J. 1997, MNRAS, 289, 869
Prieto, J. L., Chen, P., Dong, S., et al. 2020, ApJ, 889, 100
Rajamuthukumar, A. S., Hamers, A. S., Neunteufel, P., Pakmor, R., & de Mink, S. E. 2023, ApJ, 950, 9
Riess, A. G., Filippenko, A. V., Challis, P., et al. 1998, AJ, 116, 1009
Rodney, S. A., Riess, A. G., Scolnic, D. M., et al. 2015, AJ, 150, 156
Rodney, S. A., Riess, A. G., Strolger, L.-G., et al. 2014, AJ, 148, 13
Röpke, F. K., & De Marco, O. 2023, LRCA, 9, 2
Ruiter, A. J., Belczynski, K., & Fryer, C. 2009, ApJ, 699, 2026
Ruiter, A. J., Belczynski, K., Sim, S. A., Seitenzahl, I. R., & Kwiatkowski, D. 2014, MNRAS, 440, L101
Ruiz-Lapuente, P. 2023, FrASS, 10, 1112880
Ruiz-Lapuente, P., Comeron, F., Méndez, J., et al. 2004, Natur, 431, 1069
Ruiz-Lapuente, P., Damiani, F., Bedin, L., et al. 2018, ApJ, 862, 124
Ruiz-Lapuente, P., González Hernández, J. I., Cartier, R., et al. 2023, ApJ, 947, 90
Ruiz-Lapuente, P., González Hernández, J. I., Mor, R., et al. 2019, ApJ, 870, 135
Sand, D. J., Amaro, R. C., Moe, M., et al. 2019, ApJL, 877, L4
Sand, D. J., Graham, M. L., Botyánszki, J., et al. 2018, ApJ, 863, 24
Sand, D. J., Sarbadhicary, S. K., Pellegrino, C., et al. 2021, ApJ, 922, 21
Schaefer, B. E., & Pagnotta, A. 2012, Natur, 481, 164
Scherbak, P., & Fuller, J. 2023, MNRAS, 518, 3966
Schroder, K.-P., Pols, O. R., & Eggleton, P. P. 1997, MNRAS, 285, 696
Shappee, B. J., Piro, A. L., Stanek, K. Z., et al. 2018, ApJ, 855, 6
Shappee, B. J., Stanek, K. Z., Pogge, R. W., & Garnavich, P. M. 2013, ApJL, 762, L5
Shen, K. J., & Bildsten, L. 2007, ApJ, 660, 1444
Siebert, M. R., Dimitriadis, G., Polin, A., & Foley, R. J. 2020, ApJL, 900, L27
Silverman, J. M., Nugent, P. E., Gal-Yam, A., et al. 2013, ApJS, 207, 3
Soker, N. 2018, SCPMA, 61, 49502
Soker, N., Garcìa-Berro, E., & Althaus, L. G. 2014, MNRAS, 437, L66
Soker, N., Kashi, A., Garcìa-Berro, E., Torres, S., & Camacho, J. 2013, MNRAS, 431, 1541
Spillane, T., Raiola, F., Rolfs, C., et al. 2007, PhRvL, 98, 122501
Sternberg, A., Gal-Yam, A., Simon, J. D., et al. 2011, Sci, 333, 856
Toonen, S., Claeys, J. S. W., Mennekens, N., & Ruiter, A. J. 2014, A&A, 562, A14
Toonen, S., & Nelemans, G. 2013, A&A, 557, A87
Toonen, S., Perets, H. B., & Hamers, A. S. 2018, A&A, 610, A22
Tout, C. A. 2005, in ASP Conf. Ser. 330, The Astrophysics of Cataclysmic Variables and Related Objects, ed. J. M. Hameury & J. P. Lasota (San Francisco, CA: ASP), 279
Tucker, M. A., Ashall, C., Shappee, B. J., et al. 2022, ApJL, 926, L25
Tucker, M. A., Shappee, B. J., Vallely, P. J., et al. 2020, MNRAS, 493, 1044
Tucker, M. A., Shappee, B. J., & Wisniewski, J. P. 2019, ApJL, 872, L22
Vallely, P. J., Fausnaugh, M., Jha, S. W., et al. 2019, MNRAS, 487, 2372
Wang, B., Chen, X., Meng, X., & Han, Z. 2009, ApJ, 701, 1540
Wang, B., Justham, S., & Han, Z. 2013, A&A, 559, A94
Wang, B., Meng, X., Liu, D. D., Liu, Z. W., & Han, Z. 2014, ApJL, 794, L28
Wang, B., Podsiadlowski, P., & Han, Z. 2017, MNRAS, 472, 1593
Webbink, R. F. 1988, in IAU Coll. 103: The Symbiotic Phenomenon, ed. J. Mikolajewska et al. (Cambridge: Cambridge Univ. Press), 311
Webbink, R. F., & Iben, I. J. 1987, in IAU Coll. 95: Second Conference on Faint Blue Stars, ed. A. G. D. Philip, D. S. Hayes, & J. W. Liebert (Cambridge: Cambridge Univ. Press), 445
Whelan, J., & Iben, I. J. 1973, ApJ, 186, 1007
Williams, S. C., Hook, I. M., Hayden, B., et al. 2020, MNRAS, 495, 3859
Wiseman, P., Sullivan, M., Smith, M., et al. 2021, MNRAS, 506, 3330
Wolf, W. M., Bildsten, L., Brooks, J., & Paxton, B. 2013, ApJ, 777, 136
Zorotovic, M., Schreiber, M. R., Gänsicke, B. T., & Nebot Gómez-Morán, A. 2010, A&A, 520, A86